Geophysical Research Letters

RESEARCH LETTER
10.1029/2020GL092183

Seismological Structures on Bimodal Distribution of Deep Tectonic Tremor

Yasunori Sawaki[1], Yoshihiro Ito[2], Kazuaki Ohta[3], Takuo Shibutani[2], and Tomotaka Iwata[2]

[1]Graduate School of Science, Kyoto University, Kyoto, Kyoto, Japan, [2]Disaster Prevention Research Institute, Kyoto University, Uji, Kyoto, Japan, [3]Earthquake and Tsunami Research Division, National Research Institute for Earth Science and Disaster Resilience, Tsukuba, Ibaraki, Japan

Key Points:

- Multi-band receiver functions from global and regional deep events provide detailed plate-interface structures in the Kii Peninsula
- High-frequency images show a clear depth dependence for the subducting plate interface
- Along-dip difference in overriding plate materials and permeability explains bimodal distribution of tectonic tremor

Supporting Information:

Supporting Information may be found in the online version of this article.

Correspondence to:

Y. Sawaki,
sawaki.yasunori.87a@st.kyoto-u.ac.jp

Citation:

Sawaki, Y., Ito, Y., Ohta, K., Shibutani, T., & Iwata, T. (2021). Seismological structures on bimodal distribution of deep tectonic tremor. *Geophysical Research Letters*, *48*, e2020GL092183. https://doi.org/10.1029/2020GL092183

Received 17 DEC 2020
Accepted 30 MAR 2021

Abstract Deep tectonic tremors occur at the downdip extent of the seismogenic zone due to fluid processes. Beneath the northeastern Kii Peninsula, southwestern Japan, there is an along-dip bimodal distribution of tremor. However, no constraint exists on the structures controlling that distribution. We extract detailed seismological structures from multi-band receiver functions and evaluate conditional differences in the distribution. To achieve high resolution images along the plate interface, we utilize records of regional deep-focus earthquakes from the Pacific slab. Cross-section images show the subducting oceanic plate with depth-dependent phases along the bimodal distribution, revealing a conspicuous plate interface at the updip portion and an inconspicuous interface below the mantle wedge at the downdip portion. This indicates that episodic tremors occur in the high pore-fluid plate interface below the impermeable forearc crust, and that continual tremors occur at the permeable mantle wedge corner, owing to continuous fluid supply from the oceanic crust.

Plain Language Summary Deep slow earthquakes have mainly been detected at the deeper extent of estimated large-slip regions of large-scale regular earthquakes in the Nankai subduction zone, southwestern Japan. Epicenters of tectonic tremors are also downdip-aligned. However, some clusters of continual tremor with frequent small bursts were found at further downdip portions beneath the northeastern Kii Peninsula. The complexity of the bimodal tremor distribution poses a structural question regarding whether the tectonic tremor occurs below a mantle wedge or below the continental crust. We utilize a receiver function method that surveys subsurface velocity boundaries and evaluate detailed seismological structures around the plate interface using a multi-band analysis. Furthermore, regional deep-focus earthquake records are effectively utilized for receiver function mapping. The high-frequency cross section exhibits depth dependence of plate-interface phases, which demarcates active regions of updip events and downdip continual tremor, thus revealing that episodic tremor occurs below the continental crust and continual tremor occurs at the mantle wedge corner. The high-contrast updip interface reveals that a large amount of fluid is confined at the plate interface below the impermeable forearc crust, which may lead to active episodic slow earthquakes at updip portions.

1. Introduction

Investigation of detailed seismological structures around the subducting plate interface is essential for constraining mechanisms of megathrust and slow earthquakes. Increasing numbers of seismic networks, such as the high-sensitivity seismograph network (Hi-net, National Research Institute for Earth Science and Disaster Resilience (NIED, 2020)), have contributed to significant findings and the detection of slow earthquakes, such as low-frequency tremor (e.g., Obara, 2002), low-frequency earthquakes (LFE, Katsumata & Kamaya, 2003; Ohta & Ide, 2011), very-low-frequency earthquakes (VLFE, e.g., Ito et al., 2007), and slow-slip events (SSE, e.g., Nishimura et al., 2013; Ozawa et al., 2001; Sekine et al., 2010). The coupled phenomena of seismic tremor and SSEs are referred to as episodic tremor and slip (ETS, Obara et al., 2004; Rogers & Dragert, 2003).

Many LFEs and ETS have occurred at the deep plate interface (e.g., Shelly et al., 2006), aligning along depth contours of about 30 km in the Nankai (southwestern Japan) and Cascadia (Canada and USA) subduction zones. In the Tokai region (Nankai), high Poisson's ratios identified around an SSE zone indicate that

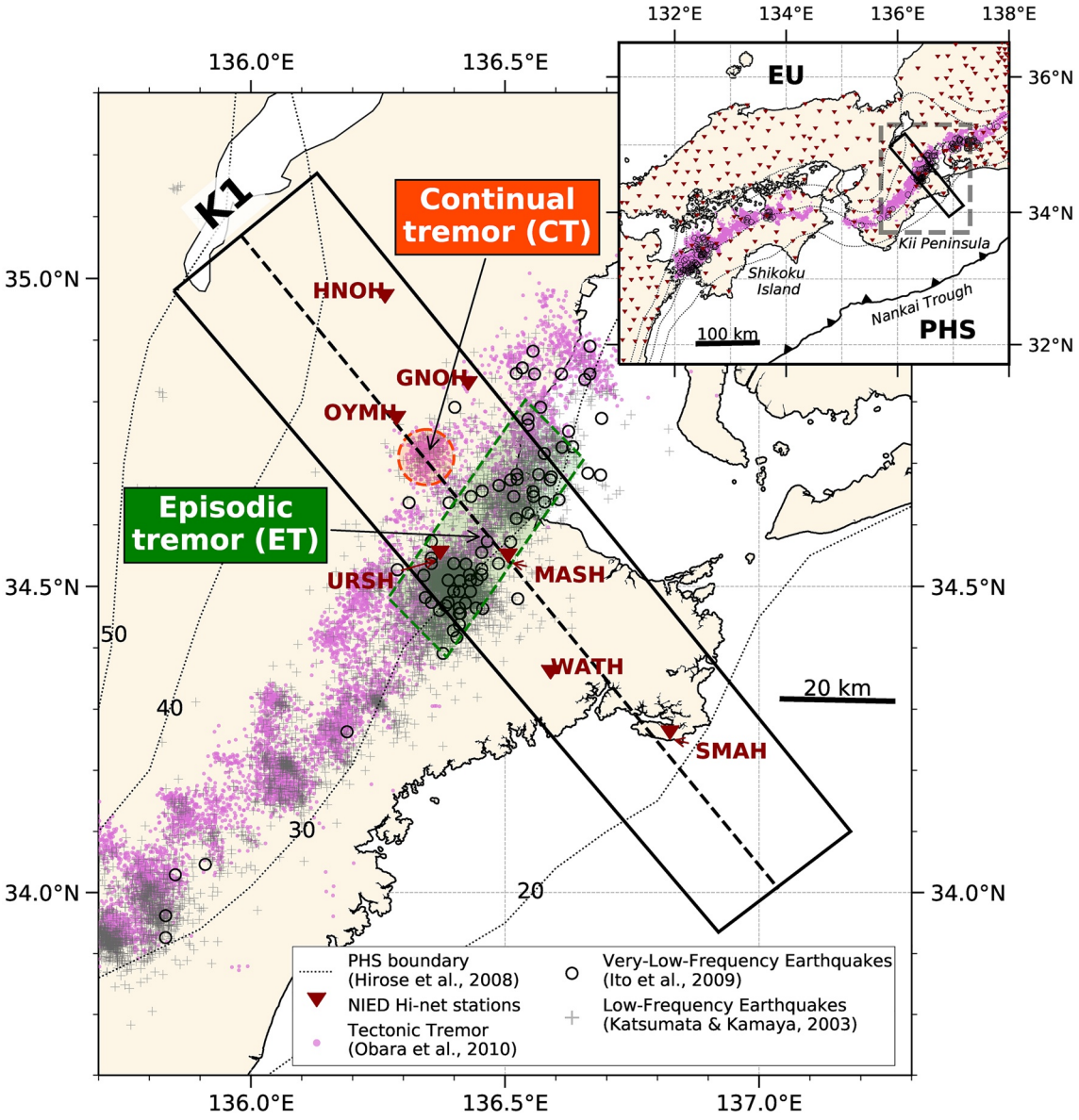

Figure 1. Maps of the Nankai subduction zone and northeastern Kii Peninsula (NE-Kii). The boxed region K1 denotes the study area used for creating cross-section receiver functions (RF) images. Purple dots are the epicenters of tectonic tremor (Maeda & Obara, 2009; Obara et al., 2010). The black circles denote epicenters of very-low-frequency earthquake (VLFE) estimated by Ito et al. (2009). The gray crosses are epicenters of low-frequency earthquake (LFE) (Katsumata & Kamaya, 2003). We define the episodic tremor as occurring in the region within the green box and the continual tremor in the region within the orange circle (Obara et al., 2010). Philippine Sea (PHS) and EU correspond to the PHS plate and the Eurasian plate, respectively. Black dashed lines are the depth contours of the PHS–EU boundary (Hirose et al., 2008).

pore-fluid pressure is high in the subducting crust (e.g., Kodaira et al., 2004), and LFEs were located beneath the mantle wedge corner due to the fluid infiltration into the wedge corner (Kato et al., 2010). In Cascadia, however, some LFEs and tremors are located shallower than the forearc Moho (e.g., Kao et al., 2009; Plourde et al., 2015; Royer & Bostock, 2014) and are thought to occur around the forearc crust by updip fluid transport with quartz precipitation (Hyndman et al., 2015; McCrory et al., 2014). In both cases, fluid transport properties are key factors of slow earthquakes around the deep plate interface (e.g., Peacock et al., 2011).

In Nankai, the oceanic Philippine Sea (PHS) plate is subducting beneath the continental Eurasian plate along the Nankai trough (Figure 1), for which multiple models of the PHS plate have been proposed using

active or passive sources (e.g., Baba et al., 2002; Hirose et al., 2008; Matsubara et al., 2008). One of the most powerful methods to identify the geometry of the subducting plate is using receiver functions (RF; Ammon, 1991), which can extract *P*-to-*S* converted waves on subsurface velocity boundaries, and identify oceanic slab geometry by identifying the oceanic Mohorovičić discontinuity (Moho) or the subducting plate interface. Shiomi et al. (2008) calculated low-frequency RFs (<0.6 Hz) and constrained the oceanic Moho shape in Nankai and found that most of the tremor epicenters were distributed along isodepth contours of the plate interface beneath the Kii Peninsula and Shikoku island at a depth of 33 ± 3 km (Figure 1). This implies that tectonic tremor would occur under similar pressure conditions across the entire tremor source area, assuming that all tremors occurred along the subducting plate interface (e.g., Shelly et al., 2006).

Recent studies of high-frequency RFs have identified a low-velocity layer in the upper oceanic crust in Nankai, which is in a highly hydrous state (e.g., Akuhara et al., 2017; Akuhara & Mochizuki, 2015). Beneath the Kii Peninsula, the basaltic oceanic crust subducts to a depth of 50 km and is a low-velocity layer (Hori et al., 1985). Akuhara et al. (2017) determined the thickness of the low-velocity layer to be less than 1–2 km at depths of around 20 km and revealed the presence of a fluid-rich sediment layer beneath the overriding plate. In Cascadia, Audet et al. (2009) showed a strong negative velocity contrast at the top of the oceanic crust extending downdip to the region of ETS beneath a lower continental crust. Besides, mafic gabbro rocks that constitute the lower forearc crust have a permeability of around two orders of magnitude lower than that of the serpentinite that is altered from the mantle peridotite (Katayama et al., 2012) and prevent geofluid from migrating upward (Audet et al., 2009; Peacock et al., 2011). Thus, the strong velocity contrast at the subducting interface is also representative of a low-permeability seal of overlying crust capable of raising pore-fluid pressures to near-lithostatic conditions along the plate interface, which may enable ETS at depths up to 35 km (Peacock et al., 2011).

A significant finding of tremor distribution has been made by Obara et al. (2010) in that an along-dip bimodal distribution of tectonic tremor was identified in the northeastern Kii Peninsula (NE-Kii), namely: an updip episodic tremor and a downdip continual tremor along the plate interface (Figure 1). The updip tremor is laterally aligned along the isodepth plate interface and comprises bursts of tremor accompanied by geodetically detectable SSEs (episodic tremor). In contrast, continual downdip tremor activity is distributed in isolated small clusters at the downdip portion from the observed area of episodic events along the plate interface. Most of the epicenters for VLFEs and LFEs are located in the same area as that of episodic tremor at the updip and few are in the area of continual tremor at the downdip (Ito et al., 2009; Katsumata & Kamaya, 2003). Obara et al. (2010) also implied that continuous stress accumulation at the boundary between the free-sliding and the transition zones could be the cause of continual tremor, However, no constraint of seismological structures on bimodal tremor activities has been achieved.

Seismological structures capable of hosting slow earthquakes are still under debate, and structural conditions of bimodal tremor activities in NE-Kii are not well understood in that it is unclear as to which seismological structures host the tremors—the interface between oceanic and continental crusts, or the interface between the oceanic crust and mantle wedge material. Estimating the seismological structure around the source region of slow earthquakes will be highly beneficial toward constraining the generation mechanisms of such slow earthquakes and megathrust earthquakes. Therefore, we herein perform a multi-band RF analysis including regional deep-focus event records and show the seismological structure in high detail by targeting the source regions of ETS to estimate the characteristics of bimodal tremor emerging around the plate boundary.

2. Methods

2.1. Multi-Band Receiver Function Analysis

The RF method has been widely used to study the velocity discontinuity structures beneath seismic stations. Gaussian low-pass filters are usually applied to avoid numerical instability on the deconvolution operation, but the depth resolution with RF is attributed to the frequency contents of incident waves because high-frequency waveforms with shorter *S*-wave wavelengths λ_S will reveal smaller-scale structures (e.g., Cassidy, 1992; Levin et al., 2016). Levin et al. (2016) introduced the vertical separation h between two vertically

propagating *P*-to-*S* converted waves from horizontal boundaries as $h = \frac{\lambda_S}{4}\left(\frac{\alpha}{\alpha - 1}\right) \sim 0.58\lambda_S$, for the ratio of *P* and *S*-wave velocities $\alpha = 1.75$. Assuming the general corner frequency of 0.6 Hz, the separation is around 3.6 km for the *S*-wave velocity of 3.7 km/s. We note that the resolution of 3.6 km is not sufficiently high to investigate detailed seismological structures around ETS activities considering the thrusting on the plate interface (Shelly et al., 2006) with confined shear zones, although it is sufficient to obtain phases of the oceanic Moho discontinuity and the plate interface. Therefore, we calculate RFs with two different corner frequencies of 0.6 and 2 Hz and refer to this approach as multi-band RF analysis. We use the low-frequency RFs to identify primary structures and the broader-band RFs for detailed structures. RFs are calculated by the extended-time multitaper (Figure S1) technique (Helffrich, 2006; Shibutani et al., 2008), which was designed to carry out impartial estimation in RF amplitudes for the entire duration of the analyzed waveform (supporting information Text S1).

We investigate seismological structures of the subducting PHS plate and the overriding plate using seismic recordings of *P*-coda waves from teleseisms and regional deep-focus earthquakes. The direct *P* and the *P*-coda waves are recorded in the first portion of a teleseismic seismogram with the epicentral distance between 30° and 90°, mainly in the vertical component due to the near-vertical incidence (Figure 2a and Figure S2).

2.2. Regional Deep-Focus Earthquakes in the Pacific Slab

Beneath southwestern Japan, two oceanic plates are presently subducting below the Eurasian plate. One is the PHS plate, subducting just below the Eurasian plate and causing a relatively large number of ordinary earthquakes and several types of slow earthquakes by interacting with the overriding continental plate. The other is the Pacific (PAC) plate, subducting further below the PHS plate at a greater angle. Many deep-focus intraplate earthquakes are occurring in the PAC at the Izu-Bonin subduction zone (Figure 2b) and showing the double seismic zone (e.g., Iidaka & Furukawa, 1994), while epicenters of deep-focus earthquakes are aligned linearly from northwest to southeast. Generally, the regional-distance earthquakes should be excluded from the RF analysis because their seismic signals contain reverberation phases (e.g., Park & Levin, 2001). However, since rays from regional deep-focus earthquakes propagate in more vertical fashions to the surface, ray-paths of regional deep events can more closely resemble those of teleseismic events, as used in RF analysis.

Southwestern Japan is a suitable region with available seismic records of regional deep-focus earthquakes for application to the multi-band RF analysis. A large number of deep-focus earthquakes in the PAC slab regularly occur below the Kii Peninsula at depths of more than 200 km (Figure 2b). Ray slowness values of regional deep earthquakes are not very different from those of ordinary teleseismic events (Figure S2). In fact, seismograms of radial and vertical components resemble each other (Figure S4), which demonstrates that we can calculate RFs from regional deep earthquakes as teleseismic RFs. Furthermore, the regional deep events tend to occur closer to seismic stations than teleseismic events. Thus, waveforms suffer less energy loss by the attenuation effect at higher frequencies. With higher signal-to-noise ratios than teleseismic seismograms at the same magnitude, we can raise the number of traces used in RF analysis, owing to the regional deep-event records with smaller magnitudes. Notably, deep-focus earthquakes occurring under the Kii Peninsula are distributed linearly from the northwest to the southeast, which is similar to the dip azimuth of the PHS plate (Hirose et al., 2008) (Figures 1 and 2b). Thus, we took advantage of the linear distribution of such deep earthquakes for the two-dimensional (2D) mapping along the dip direction of the PHS plate.

3. Data

We used three-component seismograms of regional deep-focus events and teleseisms, observed at Hi-net boreholes. In this study, a regional deep-focus earthquake was defined by an event that occurred in the PAC slab deeper than 200 km and within the epicentral distance of 10°. Based on this definition, we selected 74 regional deep-focus events with epicentral distances up to 10° and magnitudes over 5.3 from February 2005 to December 2018 (Figure 2b), following selection procedures (supporting information Text S2). We also

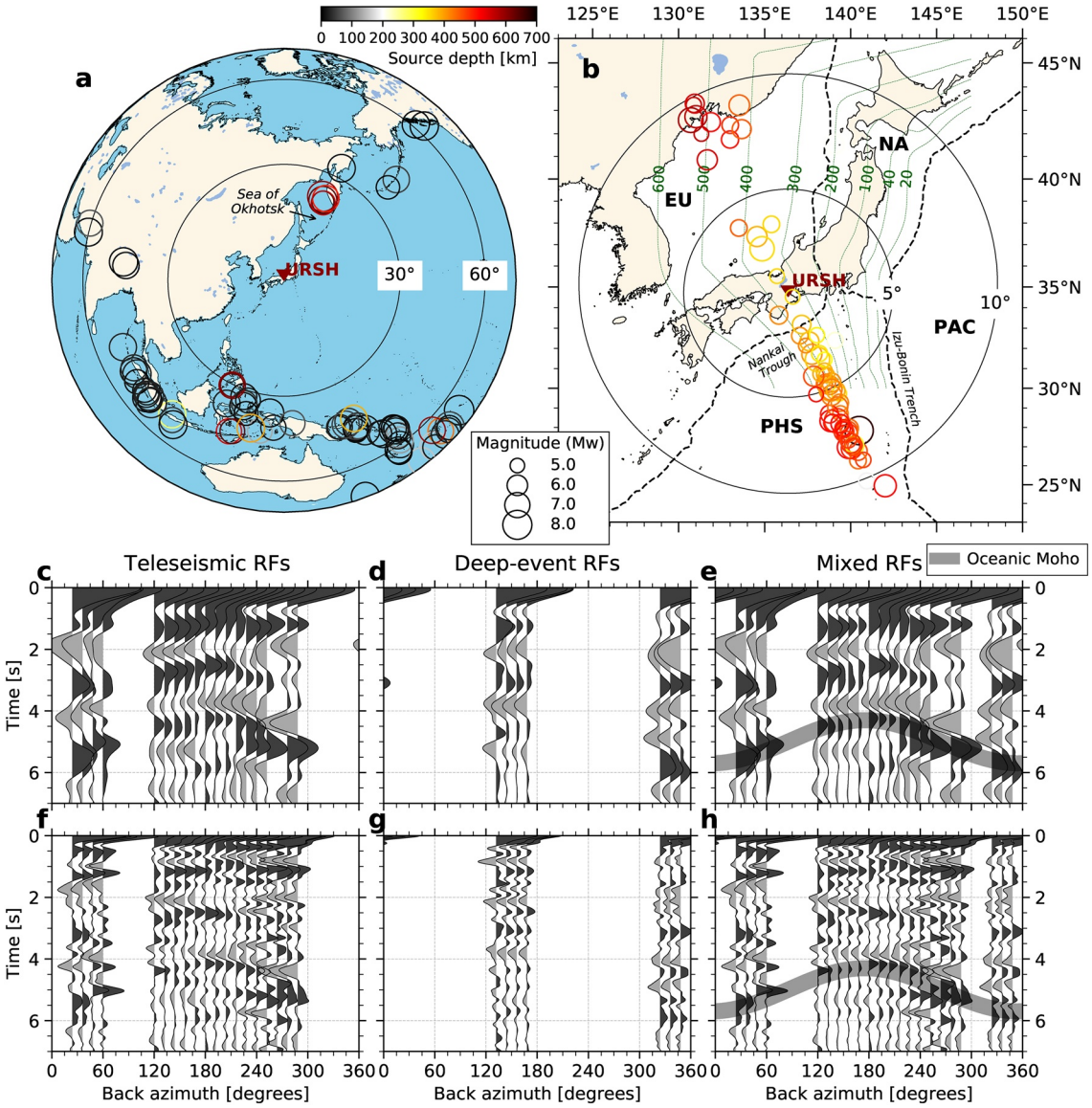

Figure 2. Hypocenters of (a) teleseismic and (b) regional deep-focus earthquake events over 200 km depth in the Pacific plate (PAC) used in this analysis, and stacked radial receiver functions (RFs) sorted with back azimuths at the station marked URSH in NE-Kii, up to 0.6 Hz (c–e) and 2.0 Hz (f–h). The radius and the edge color of each circle plot shows the seismic moment magnitude and the source depth, respectively (a and b). The green dashed lines denote the depth contour of the PAC slab (Kita et al., 2010; Nakajima et al., 2009; Nakajima & Hasegawa, 2006). PHS, PAC, NA, and EU correspond to the Philippine Sea (PHS) plate, the Pacific plate (PAC), the North American plate and the Eurasian plate, respectively. (c and f) Teleseismic RFs with events shown in (a). (d and g) RFs using regional deep-focus event records (b). (e and f) Mixed and stacked RFs of both kinds of events. Horizontal and vertical axes denote the back azimuth [degrees] and delay time [s], respectively. Positive and negative phases are shaded with dark and light gray, respectively. The oceanic Moho phases are indicated as thick gray lines. Each trace is stacked from those in back azimuth bins, whose widths and intervals are 12° and 24°, respectively, and are plotted if no less than three original traces are in each bin.

selected 78 teleseisms located at the epicentral distance from 30° to 90° with magnitudes over 6.6 from January 2006 to July 2015 (Figure 2a). Events that occurred far below the Sea of Okhotsk within the epicentral distance of ~23° were included in teleseisms because multiple phases for *P* waves did not appear when the source depth was near or over 500 km depth and the epicentral distance was greater than 22° (Figures S3d–S3f). We applied a bandpass filter from 0.05 to 50 Hz when removing the instrumental response and corrected the horizontal components using sensor orientation values estimated by NIED.

4. Results

4.1. Comparison of Stacked Receiver Function Traces

We calculated teleseismic and regional deep-event RFs for a set of locations on NE-Kii (Figures 2c–2h and Figures S5–S10). Teleseismic RFs show two significant phases: positive phases around 4.5–5.5 s and negative phases around 4 s of lapsed time from initial *P*-wave arrivals (Figures 2c and 2f), which correspond to depths of around 36–44 and 32 km, respectively. The depths at the *P*–*S* converting point for positive and negative phases were consistent with those of the oceanic Moho (Shiomi et al., 2008) and the plate interface (Hirose et al., 2008), respectively. The positive phases around 3.5–4 s (28–32 km depth) suggest a continental Moho (Figures S5, S6, and S8). RFs from regional deep events only (hereafter deep-event RFs) were clustered in narrow ranges of back azimuth (Figures 2d and 2g, Figure S2). The deep-event RFs from 132° to 168° in back azimuth show clear negative phases around 3.7 s, similar to teleseismic RFs, indicating the presence of the PHS interface. However, the deep-event RFs from 324° to 348° in back azimuth that were characteristic of deep-focus events exhibited an unidentified split in negative phases around 4–5 s and very deep oceanic Moho phases around 6 s. RFs including both the teleseismic and deep-focus events (hereafter mixed RFs) improved the coverage of back azimuth, and the oceanic Moho phases with positive amplitudes show back-azimuthal dependency of delay time and amplitude (Figures 2e and 2h). Shiomi and Park (2008) verified the relationship between the back azimuth dependency and a dipping structure of the conversion plane. Our result implies a north-dipping oceanic Moho, which represents northward dipping when compared with the oceanic Moho geometry by Shiomi et al. (2008) (Figure S11). Furthermore, broader-band RFs (2 Hz) exhibited many sharp phases compared with the low-frequency RFs (0.6 Hz). At downdip for back azimuth from 252° to 36°, the oceanic Moho phases split into two or three peaks, while the PHS boundary phases merely sharpened. The time separation of two peaks on the high-frequency RFs corresponds to a depth difference of ∼1 km. Thus, the simple sharp phases from the PHS boundary represent a sharp velocity transition on a thin subduction interface (<1 km thickness), while splitting on the oceanic Moho phases implies a gradual downward velocity increase with a thick oceanic Moho (2–3 km thickness; Nedimović et al., 2005).

4.2. Cross-Section Image

We estimated subsurface structures from a two-dimensional cross-section of multi-band RFs along a survey line, which crosses the source regions of episodic tremor and continual tremor (Figure 3). We applied common-conversion-point (CCP) stacking of RFs to obtain cross-section images—a back-projection method in which RF amplitudes are properly plotted along a depth-converted raypath. We used the JMA2001 one-dimensional velocity model (Ueno et al., 2002) for the depth conversion. The corner frequencies of 0.6 Hz (low frequency) and 2 Hz (high frequency) were selected for comparing the cross-section derived from mixed RFs to that from teleseismic RFs. The conventional low-frequency image from teleseismic RFs (Figure 3b) shows a positive signal of the continental Moho at 30 km depth ($X > 20\left[\mathrm{km}\right]$) and a continuous positive phase dipping in the northwest direction at 30–50 km depth, which is over 5 km deeper than the depth contour of the plate interface (Hirose et al., 2008). This demonstrates the velocity increase at the oceanic Moho from the crust to the mantle. A negative phase dipping to the northwest at 20–45 km depth shows the plate interface. However, this phase is discontinuous. The narrow range of incident angles for teleseismic rays led to the lateral discontinuity of target phases.

In contrast, low-frequency images, including deep-event RFs (Figure 3c), show more continuous and conspicuous phases than the ordinary RFs using only teleseismic data (Figure 3b). The negative dipping phase is the PHS interface, which is consistent with the isodepth contours of the plate interface (Hirose et al., 2008). Deep-event RFs with a wider range of slowness and an aligned distribution of events contribute to the clarification of phases by widening the range of trace packets under each seismic station and filling more grids during the CCP stacking procedure. A well-imaged oceanic Moho with positive amplitudes was confirmed at $-50 < X\ [\mathrm{km}] < 50$ by the improved continuity of RF phases showing the oceanic plate.

High-frequency RFs (Figure 3d) show the negative phases for the plate interface, which were notably clear and sharp up to 35 km depth ($-30 < X\left[\mathrm{km}\right] < 15$ along the cross-section) and less clear at the deeper por-

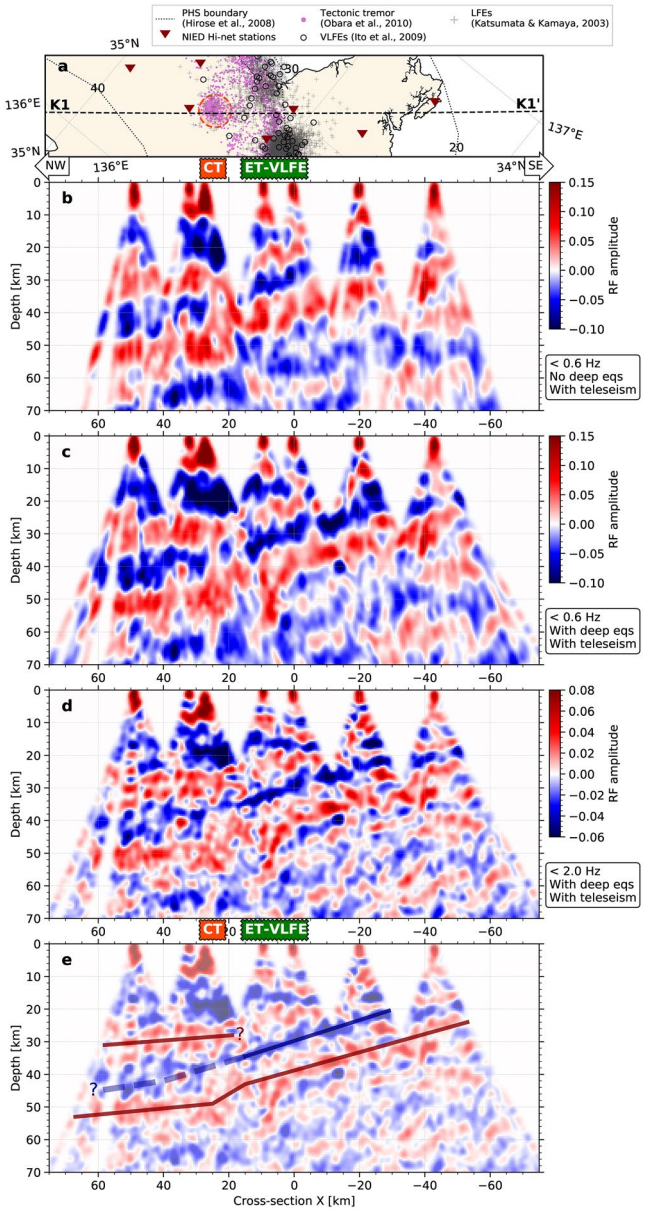

Figure 3. Two-dimensional cross-section images of radial multi-band receiver functions (RF) along the line K1 in Figure 1. (a) A map showing stations (reversed triangle) and tremor (gray) along the line K1 (dashed line). (b) Teleseismic low frequency (<0.6 Hz) RF images. (c and d) RFs including regional deep-focus earthquakes, for frequencies up to (c) 0.6 Hz and (d) 2 Hz. (e) The interpretation of RF phases for (d). The horizontal axis denotes the cross-section distance X [km] along the line K1, shared in (b–d). The vertical axis denotes the depth conversion of each trace from the delay time by 2D stacking method. The purple dots denote epicenters of tectonic tremor from the NIED catalog (Maeda & Obara, 2009; Obara et al., 2010). The black circles denote epicenters of very-low-frequency earthquake (VLFE) estimated by Ito et al. (2009). The gray crosses are epicenters of LFE (Katsumata & Kamaya, 2003). ET and CT are abbreviations of the episodic tremor and the continual tremor. The JMA2001 1D velocity model (Ueno et al., 2002) is applied in depth conversion. If a seismic station is over 10 km distant from the *Ps* conversion point, the RF amplitude was attenuated in response to the distance. The grid size is 0.5 × 0.5 km, and the Gaussian smoothing parameter σ is 1.5 km.

tions ($X > 15$ [km]). The interpretation of each phase is shown in Figure 3e. The depth-dependent plate interface with negative amplitudes (blue) is observed along with the oceanic or continental Moho with positive amplitudes (red). In general, RF amplitudes are dependent on the shear-wave velocity contrast (Audet et al., 2009) and the sharpness of the boundary thickness (Levin et al., 2016; Li et al., 2017). These

results demonstrate a strong velocity contrast in a narrow region at the updip interface and a gradual velocity transition in the mantle wedge from the downdip interface to the continental Moho.

Interestingly, the depth-dependent image of the plate interface demarcates active regions of updip episodic events and downdip continual tremor (Figure 3e). The plate interface with strong negative amplitudes lies beneath most of the epicenters for episodic tremor—LFEs and VLFEs ($-5 < X\left[\mathrm{km}\right] < 15$). However, the cross-section distance for epicenters of continual tremor corresponded to the entry point into the unclear interface around the horizontal distance of 20–30 km, indicating the mantle wedge.

5. Discussion

5.1. Tremor in the Crust–Crust Zone

The broader-band RF image (Figure 3e) shows the negative phases for the plate interface, which is clear and sharp up to 35 km depth ($-30 < X\left[\mathrm{km}\right] < 15$ along the cross-section) and less clear at the deeper portions ($X > 15$ [km]). The distinctively conspicuous phase of the updip interface confirms that the upper oceanic crust is in a highly hydrous state, as previous studies have noted (e.g., Akuhara & Mochizuki, 2015; Kato et al., 2010). The sharper phase with a strong negative amplitude at the shallower portion shows that the seismic velocity steeply drops from forearc to oceanic crusts within a narrow area, which indicates a low-velocity layer in a hydrous state at the uppermost oceanic crust. Sediments would likely undergo compaction at depths less than 20 km (Hyndman & Peacock, 2003). Therefore, the sharp phase of the plate interface may not be associated with the possible existence of the fluid-rich sediment layer (Akuhara et al., 2017). A more plausible cause of the sharp phase is the basaltic oceanic crust (Hori et al., 1985; Hyndman & Peacock, 2003). If the potentially large velocity contrast at the thin subducting interface represents the presence of near-lithostatic pore-fluid pressures (Audet et al., 2009), the over-pressured basaltic oceanic crust should likely extend to depths of 35 km depth beneath NE-Kii as well as beneath Cascadia (Peacock et al., 2011).

The depth variation of high-frequency RFs can be interpreted as the difference in the permeability along the plate interface, and it is likely that the strong negative phase at the updip portion represents a low-permeability interface (e.g., Audet et al., 2009). The low-permeability seal probably causes an increase in pore-fluid pressures on the plate interface, which could lead to the high level of activity of short-term SSEs or LFEs (Nakajima & Hasegawa, 2016; Nishimura et al., 2013) in NE-Kii. Hypocenters of LFEs are well mapped at the upper oceanic crust (Figure 4), which is nearly consistent with the assumption that LFEs occur near plate interfaces (Shelly et al., 2006). Episodic tremor also occurs around the interface between the continental crust and oceanic crust under the condition that sufficient geofluid is confined, thereby assuming that the tremor comprises a swarm of LFEs (Shelly et al., 2007). High tremor energy rates and the large slip amount of SSEs in NE-Kii (Yabe & Ide, 2014) may support the hypothesis that frequent short-term SSEs break the permeability seal and allow for abundant built-up fluid along the interface to migrate upward, leading to tremor generation (e.g., Gosselin et al., 2020; Nakajima & Uchida, 2018).

5.2. Tremor in the Crust–Mantle Area

In contrast, downdip continual tremor corresponds to the mantle wedge region with the broad image of the plate interface (Figure 3). The decrease in amplitude of the broad phases of the slab interface at the downdip portion shows that the velocity transition is gradual at the mantle wedge corner. When taking into account that the permeability of the mantle peridotite is higher than that of the crustal gabbro (Katayama et al., 2012), the higher permeability of the slab interface is facilitated (e.g., Audet et al., 2009). This indicates the mantle wedge is in a hydrous state due to fluid drainage from the plate boundary and produces serpentinite (e.g., Hacker et al., 2003). Thus, we believe that a possible source region of the continual tremor is the partially serpentinized mantle wedge corner. Obara et al. (2010) mentioned that the continuous stress concentration and weak frictional strength at the boundary between the free-sliding and the transition zones at the wedge corner may cause activation of continual tremor. Assuming the fluid source is the eclogitization of the oceanic crust at the deeper portion (e.g., Hacker et al., 2003), the slab-derived fluid is stably supplied into the shallower part of the mantle wedge. Thus, the continuous supply of fluid

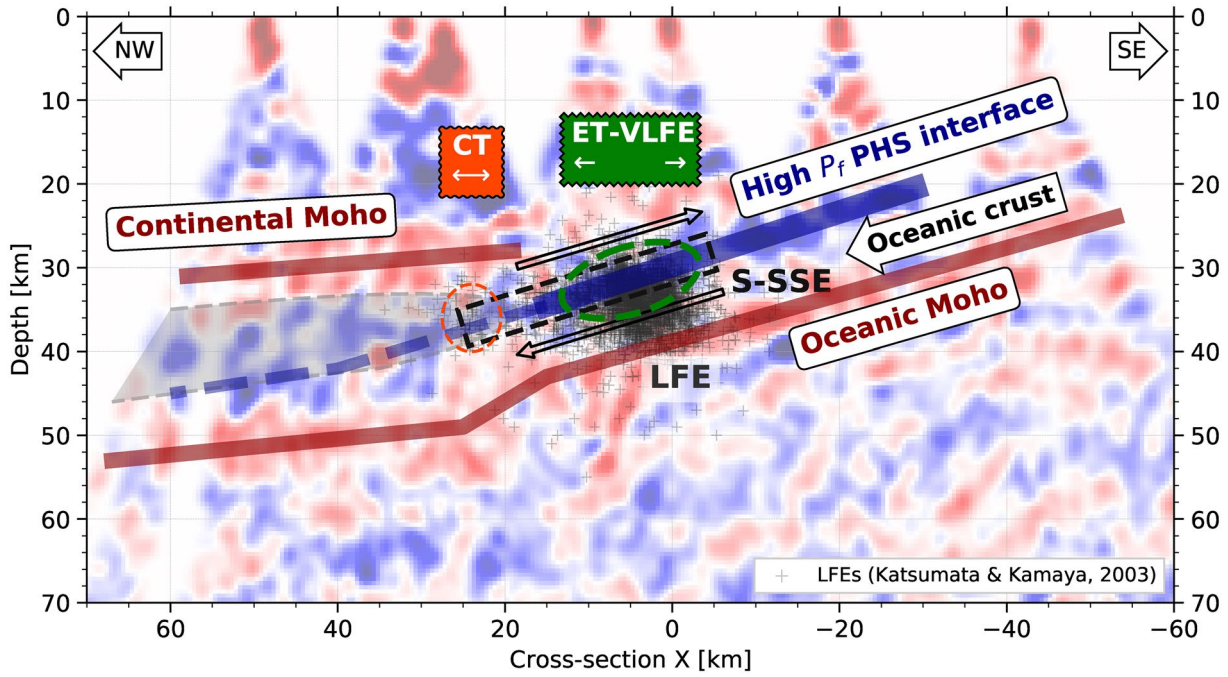

Figure 4. Schematic depth view of slow earthquake activities and underground structures around the Philippine Sea (PHS) interface beneath NE-Kii. Gray crosses are hypocenters of low-frequency earthquakes (LFEs) (Katsumata & Kamaya, 2003). The green ellipse denotes assumed regions where episodic tremor and very-low-frequency earthquakes (VLFEs) occurred. The orange ellipse denotes assumed regions of continual tremor. The black rectangle shows the region of the largest slip amount for short-term slow-slip events (SSEs) (Nishimura et al., 2013).

to the wedge corner could cause continual tremor activities. If a large volume of mantle wedge can be hydrated, the pore-fluid pressure is unlikely to rise suddenly, which would account for minor and continual activities.

5.3. Comparison with Cascadia and Prospects for Spatio-Temporal Variations

In Cascadia, Wech and Creager (2011) showed gradual transitions of tremor activity from episodic to continual at greater depths, and Idehara et al. (2014) revealed some clusters of continual tremor at downdip of the tremor band. The forearc mantle corner passes through the center of the tremor band (McCrory et al., 2014), suggesting that continual tremor occurs at the wedge corner and that some of this episodic tremor could occur beneath the forearc crust in Cascadia, as well as in NE-Kii (from our results). This is because the peak occurrence of episodic tremor coincides with the mantle wedge corner (Audet et al., 2010). Unlike Tokai (Kato et al., 2010) and NE-Kii, the inverted Moho has been reported in Cascadia (e.g., Bostock et al., 2002), which may suggest that hydrous conditions at the downdip portion differ. Further observations and analyses are required to clarify the differences in geophysical properties.

Importantly, our high-frequency analysis with regional deep events contributes to the detection of detailed imagery of the over-pressured oceanic crust, without requiring dense-network temporal observation data. Therefore, this method may also be applied to other regions in the Nankai subduction zone, such as Tokai and Shikoku, to assess regionality. However, it should be noted that the cross-section image presents an averaged overview of the longer-term situation, rather than periodical characteristics of slow earthquake activities. Gosselin et al. (2020) illustrated the temporal variation in seismic velocity during ETS in Cascadia. However, additional teleseisms and regional deep events would be required to assess the temporal variation in structural conditions along the interface during the occurrence of slow earthquakes. In this manner, considering the use of temporal observation data may help enhance the spatial coverage. Investigating the spatio-temporal variation of RF phases is crucial for evaluating pore-fluid conditions and the occurrence of slow earthquakes or megathrusts.

6. Conclusions

We performed multi-band receiver function analysis using Hi-net seismograph records on NE-Kii, in southwestern Japan. Regional deep earthquakes that occurred in the PAC slab were used to calculate high-frequency RFs. The wider range of the rays made the cross-section images more continuous. Cross-section images of RFs revealed the subducting oceanic crust over a positive phase of the oceanic Moho, thereby illustrating a conspicuous negative phase of the plate interface in the shallower portion and an obscure structure of the mantle wedge in the deeper portion. The conspicuousness of the updip interface confirmed that the upper oceanic crust is under fluid-saturated conditions below the impermeable forearc crust. The along-dip difference of the interface phase corresponded well with the along-dip bimodal distribution of tectonic tremor observed by Obara et al. (2010). The present results imply that updip episodic tremor, LFEs, and VLFEs occur around the high pore-fluid plate interface below the impermeable continental crust, and also show that the downdip continual tremor occurs at the hydrous mantle wedge corner. This implication provides new insights into the structural diversity of slow earthquake source regions in the Nankai subduction zone. Further studies are required to assess the heterogeneity and temporal variations in seismological structures around the plate interface in response to the occurrence of short-term or long-term SSEs and episodic slow events.

Conflict of Interest

The authors declare that there are no conflicts of interest.

Data Availability Statement

The authors used seismic data from NIED Hi-net (National Research Institute for Earth Science and Disaster Resilience, 2020) and a catalog of tectonic tremors provided by NIED. Teleseismic events and regional deep-focus earthquakes were searched by the USGS Earthquake Catalog (U.S. Geological Survey, 2020, last accessed on December 2020) (https://earthquake.usgs.gov/earthquakes/search/). The authors used the Python toolbox "ObsPy" (Beyreuther et al., 2010; Krischer et al., 2015; Megies et al., 2011) to process seismological data. The authors also used the Python package "cartopy" (Elson et al., 2020) for mapping geospatial data, and all figures were created by the 2D graphics package "Matplotlib" (Hunter, 2007). The authors used the high-resolution spatial database of Global Administrative Areas (https://gadm.org/). Certain catalogs of slow earthquakes were downloaded using the "Slow Earthquake Database" (Kano et al., 2018).

Acknowledgments
The authors appreciate Katsuhiko Shiomi (NIED) for providing the PHS Moho contours (Shiomi et al., 2008). The authors also thank Vadim Levin and an anonymous reviewer for thorough reviews and constructive comments that improved this study. This research was supported by the Ministry of Education, Culture, Sports, Science and Technology (MEXT) of Japan, under its Earthquake and Volcano Hazards Observation and Research Program (JSPS KAKENHI Grant Number JP16H06472) in Scientific Research on Innovative Areas Science of Slow Earthquakes, and Science and Technology Research Partnership for Sustainable Development (SATREPS) and the Japan Science and Technology Agency (JST) with grant number JPMJSA1510.

References

Akuhara, T., & Mochizuki, K. (2015). Hydrous state of the subducting Philippine Sea plate inferred from receiver function image using onshore and offshore data. *Journal of Geophysical Research: Solid Earth*, *120*, 8461–8477. https://doi.org/10.1002/2015jb012336

Akuhara, T., Mochizuki, K., Kawakatsu, H., & Takeuchi, N. (2017). A fluid-rich layer along the Nankai trough megathrust fault off the Kii Peninsula inferred from receiver function inversion. *Journal of Geophysical Research: Solid Earth*, *122*, 6524–6537. https://doi.org/10.1002/2017jb013965

Ammon, C. J. (1991). The isolation of receiver effects from teleseismic P waveforms. *Bulletin of the Seismological Society of America*, *81*, 2504–2510. https://doi.org/10.1029/2005JB004161

Audet, P., Bostock, M. G., Boyarko, D. C., Brudzinski, M. R., & Allen, R. M. (2010). Slab morphology in the Cascadia fore arc and its relation to episodic tremor and slip. *Journal of Geophysical Research*, *115*, 1–15. https://doi.org/10.1029/2008jb006053

Audet, P., Bostock, M. G., Christensen, N. I., & Peacock, S. M. (2009). Seismic evidence for overpressured subducted oceanic crust and megathrust fault sealing. *Nature*, *457*(7225), 76–78. https://doi.org/10.1038/nature07650

Baba, T., Tanioka, Y., Cummins, P. R., & Uhira, K. (2002). The slip distribution of the 1946 Nankai earthquake estimated from tsunami inversion using a new plate model. *Physics of the Earth and Planetary Interiors*, *132*(1–3), 59–73. https://doi.org/10.1016/s0031-9201(02)00044-4

Beyreuther, M., Barsch, R., Krischer, L., Megies, T., Behr, Y., & Wassermann, J. (2010). ObsPy: A python toolbox for seismology. *Seismological Research Letters*, *81*(3), 530–533. https://doi.org/10.1785/gssrl.81.3.530

Bostock, M. G., Hyndman, R. D., Rondenay, S., & Peacock, S. M. (2002). An inverted continental Moho and serpentinization of the forearc mantle. *Nature*, *417*(6888), 536–538. https://doi.org/10.1038/417536a

Cassidy, J. F. (1992). Numerical experiments in broadband receiver function analysis. *Bulletin of the Seismological Society of America*, *82*(3), 1453–1474.

Elson, P., Andrade, E. S. de., Hattersley, R., Campbell, E., May, R., Dawson, A., et al. (2020). *SciTools/cartopy: Cartopy 0.18.0*. Zenodo. https://doi.org/10.5281/zenodo.3783894

Gosselin, J. M., Audet, P., Estève, C., McLellan, M., Mosher, S. G., & Schaeffer, A. J. (2020). Seismic evidence for megathrust fault-valve behavior during episodic tremor and slip. *Science Advances*, *6*(4), eaay5174. https://doi.org/10.1126/sciadv.aay5174

Hacker, B. R., Peacock, S. M., Abers, G. A., & Holloway, S. D. (2003). Subduction factory 2. Are intermediate-depth earthquakes in subducting slabs linked to metamorphic dehydration reactions? *Journal of Geophysical Research*, *108*(B1), 2030. https://doi.org/10.1029/2001jb001129

Helffrich, G. (2006). Extended-time multitaper frequency domain cross-correlation receiver-function estimation. *Bulletin of the Seismological Society of America*, *96*(1), 344–347. https://doi.org/10.1785/0120050098

Hirose, F., Nakajima, J., & Hasegawa, A. (2008). Three-dimensional seismic velocity structure and configuration of the Philippine Sea slab in southwestern Japan estimated by double-difference tomography. *Journal of Geophysical Research*, *113*, B09315. https://doi.org/10.1029/2007jb005274

Hori, S., Inoue, H., Fukao, Y., & Ukawa, M. (1985). Seismic detection of the untransformed 'basaltic' oceanic crust subducting into the mantle. *Geophysical Journal International*, *83*(1), 169–197. https://doi.org/10.1111/j.1365-246x.1985.tb05162.x

Hunter, J. D. (2007). Matplotlib: A 2D graphics environment. *Computer Science and Engineering*, *9*(3), 90–95. https://doi.org/10.1109/mcse.2007.55

Hyndman, R. D., McCrory, P. A., Wech, A., Kao, H., & Ague, J. (2015). Cascadia subducting plate fluids channelled to fore-arc mantle corner: ETS and silica deposition. *Journal of Geophysical Research: Solid Earth*, *120*, 4344–4358. https://doi.org/10.1002/2015jb011920

Hyndman, R. D., & Peacock, S. M. (2003). Serpentinization of the forearc mantle. *Earth and Planetary Science Letters*, *212*(3–4), 417–432. https://doi.org/10.1016/s0012-821x(03)00263-2

Idehara, K., Yabe, S., & Ide, S. (2014). Regional and global variations in the temporal clustering of tectonic tremor activity. *Earth Planets and Space*, *66*, 66. https://doi.org/10.1186/1880-5981-66-66

Iidaka, T., & Furukawa, Y. (1994). Double seismic zone for deep earthquakes in the Izu-Bonin subduction zone. *Science*, *263*(5150), 1116–1118. https://doi.org/10.1126/science.263.5150.1116

Ito, Y., Obara, K., Matsuzawa, T., & Maeda, T. (2009). Very low frequency earthquakes related to small asperities on the plate boundary interface at the locked to aseismic transition. *Journal of Geophysical Research*, *114*, 1–16. https://doi.org/10.1029/2008jb006036

Ito, Y., Obara, K., Shiomi, K., Sekine, S., & Hirose, H. (2007). Slow earthquakes coincident with episodic tremors and slow slip events. *Science*, *315*(5811), 503–506. https://doi.org/10.1126/science.1134454

Kano, M., Aso, N., Matsuzawa, T., Ide, S., Annoura, S., Arai, R., et al. (2018). Development of a slow earthquake database. *Seismological Research Letters*, *89*(4), 1566–1575. https://doi.org/10.1785/0220180021

Kao, H., Shan, S.-J., Dragert, H., & Rogers, G. (2009). Northern Cascadia episodic tremor and slip: A decade of tremor observations from 1997 to 2007. *Journal of Geophysical Research*, *114*, B00A12. https://doi.org/10.1029/2008jb006046

Katayama, I., Terada, T., Okazaki, K., & Tanikawa, W. (2012). Episodic tremor and slow slip potentially linked to permeability contrasts at the Moho. *Nature Geoscience*, *5*(10), 731–734. https://doi.org/10.1038/ngeo1559

Kato, A., Iidaka, T., Ikuta, R., Yoshida, Y., Katsumata, K., Iwasaki, T., et al. (2010). Variations of fluid pressure within the subducting oceanic crust and slow earthquakes. *Geophysical Research Letters*, *37*, 1–6. https://doi.org/10.1029/2010gl043723

Katsumata, A., & Kamaya, N. (2003). Low-frequency continuous tremor around the Moho discontinuity away from volcanoes in the southwest Japan. *Geophysical Research Letters*, *30*, 20-1–21-4. https://doi.org/10.1029/2002gl015981

Kita, S., Okada, T., Hasegawa, A., Nakajima, J., & Matsuzawa, T. (2010). Anomalous deepening of a seismic belt in the upper-plane of the double seismic zone in the Pacific slab beneath the Hokkaido corner: Possible evidence for thermal shielding caused by subducted forearc crust materials. *Earth and Planetary Science Letters*, *290*(3–4), 415–426. https://doi.org/10.1016/j.epsl.2009.12.038

Kodaira, S., Iidaka, T., Kato, A., Park, J.-O., Iwasaki, T., & Kaneda, Y. (2004). High pore fluid pressure may cause silent slip in the Nankai trough. *Science*, *304*(5675), 1295–1298. https://doi.org/10.1126/science.1096535

Krischer, L., Megies, T., Barsch, R., Beyreuther, M., Lecocq, T., Caudron, C., & Wassermann, J. (2015). ObsPy: A bridge for seismology into the scientific Python ecosystem. *Computational Science & Discovery*, *8*(1), 1–17. https://doi.org/10.1088/1749-4699/8/1/014003

Levin, V., Vantongeren, J. A., & Servali, A. (2016). How sharp is the sharp Archean Moho? Example from eastern Superior Province. *Geophysical Research Letters*, *43*, 1928–1933. https://doi.org/10.1002/2016gl067729

Li, X., Li, Z., Hao, T., Wang, S., & Xing, J. (2017). A multi-frequency receiver function inversion approach for crustal velocity structure. *Computers & Geosciences*, *102*, 45–55. https://doi.org/10.1016/j.cageo.2017.02.009

Maeda, T., & Obara, K. (2009). Spatiotemporal distribution of seismic energy radiation from low-frequency tremor in western Shikoku, Japan. *Journal of Geophysical Research*, *114*, B00A09. https://doi.org/10.1029/2008jb006043

Matsubara, M., Obara, K., & Kasahara, K. (2008). Three-dimensional P- and S-wave velocity structures beneath the Japan Islands obtained by high-density seismic stations by seismic tomography. *Tectonophysics*, *454*(1–4), 86–103. https://doi.org/10.1016/j.tecto.2008.04.016

McCrory, P. A., Hyndman, R. D., & Blair, J. L. (2014). Relationship between the Cascadia fore-arc mantle wedge, nonvolcanic tremor, and the downdip limit of seismogenic rupture. *Geochemistry, Geophysics, Geosystems*, *15*, 1071–1095. https://doi.org/10.1002/2013gc005144

Megies, T., Beyreuther, M., Barsch, R., Krischer, L., & Wassermann, J. (2011). ObsPy - what can it do for data centers and observatories? *Annals of Geophysics*, *54*(1), 47–58. https://doi.org/10.4401/ag-4838

Nakajima, J., & Hasegawa, A. (2006). Anomalous low-velocity zone and linear alignment of seismicity along it in the subducted Pacific slab beneath Kanto, Japan: Reactivation of subducted fracture zone? *Geophysical Research Letters*, *33*, 1–4. https://doi.org/10.1029/2006gl026773

Nakajima, J., & Hasegawa, A. (2016). Tremor activity inhibited by well-drained conditions above a megathrust. *Nature Communications*, *7*(13863), 1–7. https://doi.org/10.1038/ncomms13863

Nakajima, J., Hirose, F., & Hasegawa, A. (2009). Seismotectonics beneath the Tokyo metropolitan area, Japan: Effect of slab-slab contact and overlap on seismicity. *Journal of Geophysical Research*, *114*(8), 1–23. https://doi.org/10.1029/2008jb006101

Nakajima, J., & Uchida, N. (2018). Repeated drainage from megathrusts during episodic slow slip. *Nature Geoscience*, *11*(5), 351–356. https://doi.org/10.1038/s41561-018-0090-z

National Research Institute for Earth Science and Disaster Resilience. (2020). *NIED Hi-net*. https://doi.org/10.17598/nied.0003

Nedimović, M. R., Carbotte, S. M., Harding, A. J., Detrick, R. S., Canales, J. P., Diebold, J. B., et al. (2005). Frozen magma lenses below the oceanic crust. *Nature*, *436*(7054), 1149–1152. https://doi.org/10.1038/nature03944

Nishimura, T., Matsuzawa, T., & Obara, K. (2013). Detection of short-term slow slip events along the Nankai Trough, southwest Japan, using GNSS data. *Journal of Geophysical Research: Solid Earth*, *118*(6), 3112–3125. https://doi.org/10.1002/jgrb.50222

Obara, K. (2002). Nonvolcanic deep tremor associated with subduction in southwest Japan. *Science*, *296*(5573), 1679–1681. https://doi.org/10.1126/science.1070378

Obara, K., Hirose, H., Yamamizu, F., & Kasahara, K. (2004). Episodic slow slip events accompanied by non-volcanic tremors in southwest Japan subduction zone. *Geophysical Research Letters*, *31*, 1–4. https://doi.org/10.1029/2004gl020848

Obara, K., Tanaka, S., Maeda, T., & Matsuzawa, T. (2010). Depth-dependent activity of non-volcanic tremor in southwest Japan. *Geophysical Research Letters*, *37*, 1–6. https://doi.org/10.1029/2010gl043679

Ohta, K., & Ide, S. (2011). Precise hypocenter distribution of deep low-frequency earthquakes and its relationship to the local geometry of the subducting plate in the Nankai subduction zone, Japan. *Journal of Geophysical Research*, *116*, 1–11. https://doi.org/10.1029/2010jb007857

Ozawa, S., Murakami, M., & Tada, T. (2001). Time-dependent inversion study of the slow thrust event in the Nankai trough subduction zone, southwestern Japan. *Journal of Geophysical Research*, *106*(B1), 787–802. https://doi.org/10.1029/2000jb900317

Park, J., & Levin, V. (2001). Receiver functions from regional Pwaves. *Geophysical Journal International*, *147*(1), 1–11. https://doi.org/10.1046/j.1365-246x.2001.00523.x

Peacock, S. M., Christensen, N. I., Bostock, M. G., & Audet, P. (2011). High pore pressures and porosity at 35 km depth in the Cascadia subduction zone. *Geology*, *39*(5), 471–474. https://doi.org/10.1130/G31649.1

Plourde, A. P., Bostock, M. G., Audet, P., & Thomas, A. M. (2015). Low-frequency earthquakes at the southern Cascadia margin. *Geophysical Research Letters*, *42*, 4849–4855. https://doi.org/10.1002/2015gl064363

Rogers, G., & Dragert, H. (2003). Episodic tremor and slip on the Cascadia subduction zone: The chatter of silent slip. *Science*, *300*(5627), 1942–1943. https://doi.org/10.1126/science.1084783

Royer, A. A., & Bostock, M. G. (2014). A comparative study of low frequency earthquake templates in northern Cascadia. *Earth and Planetary Science Letters*, *402*(C), 247–256. https://doi.org/10.1016/j.epsl.2013.08.040

Sekine, S., Hirose, H., & Obara, K. (2010). Along-strike variations in short-term slow slip events in the southwest Japan subduction zone. *Journal of Geophysical Research*, *115*, B00A27. https://doi.org/10.1029/2008jb006059

Shelly, D. R., Beroza, G. C., & Ide, S. (2007). Non-volcanic tremor and low-frequency earthquake swarms. *Nature*, *446*(7133), 305–307. https://doi.org/10.1038/nature05666

Shelly, D. R., Beroza, G. C., Ide, S., & Nakamula, S. (2006). Low-frequency earthquakes in Shikoku, Japan, and their relationship to episodic tremor and slip. *Nature*, *442*(7099), 188–191. https://doi.org/10.1038/nature04931

Shibutani, T., Ueno, T., & Hirahara, K. (2008). Improvement in the extended-time multitaper receiver function estimation technique. *Bulletin of the Seismological Society of America*, *98*(2), 812–816. https://doi.org/10.1785/0120070226

Shiomi, K., Matsubara, M., Ito, Y., & Obara, K. (2008). Simple relationship between seismic activity along Philippine Sea slab and geometry of oceanic Moho beneath southwest Japan. *Geophysical Journal International*, *173*, 1018–1029. https://doi.org/10.1111/j.1365-246x.2008.03786.x

Shiomi, K., & Park, J. (2008). Structural features of the subducting slab beneath the Kii Peninsula, central Japan: Seismic evidence of slab segmentation, dehydration, and anisotropy. *Journal of Geophysical Research*, *113*, 1–13. https://doi.org/10.1029/2007jb005535

Ueno, H., Hatakeyama, S., Aketagawa, T., Funasaki, J., & Hamada, N. (2002). Improvement of hypocenter determination procedures in the Japan Meteorological Agency (in Japanese with English abstract). *Quarterly Journal of Seismology*, *65*, 123–134.

U.S. Geological Survey. (2020). *USGS earthquake catalog*. Retrieved from: https://earthquake.usgs.gov/earthquakes/search/

Wech, A. G., & Creager, K. C. (2011). A continuum of stress, strength and slip in the Cascadia subduction zone. *Nature Geoscience*, *4*(9), 624–628. https://doi.org/10.1038/ngeo1215

Yabe, S., & Ide, S. (2014). Spatial distribution of seismic energy rate of tectonic tremors in subduction zones. *Journal of Geophysical Research: Solid Earth*, *119*(11), 8171–8185. https://doi.org/10.1002/2014jb011383

References From the Supporting Information

Crotwell, H. P., Owens, T. J., & Ritsema, J. (1999). The TauP toolkit: Flexible seismic travel-time and ray-path utilities. *Seismological Research Letters*, *70*(2), 154–160. https://doi.org/10.1785/gssrl.70.2.154

Kennett, B. L. N., & Engdahl, E. R. (1991). Traveltimes for global earthquake location and phase identification. *Geophysical Journal International*, *105*(2), 429–465. https://doi.org/10.1111/j.1365-246X.1991.tb06724.x